Effect of microstructure on Ti_3Al precipitation during ageing of Ti-6Al-4V alloy

B. Callegari[a,b,*], J. V. Marçola[a], K. Aristizabal[b], F. A. Soldera[b], F. Mücklich[b], H. C. Pinto[a]

[a]Department of Materials Engineering, São Carlos School of Engineering, University of São Paulo, São Carlos, Brazil

[b]Chair of Functional Materials, Saarland University, Saarbrücken, Germany

*bruna2.callegari@usp.br

The aim of the present work is to explore the age-hardening potential of Ti-6Al-4V (Ti-64) alloy with variation of the starting microstructure, with attention to the precipitation of nano-sized Ti_3Al phase, as influenced by microstructural features. The alloy was either solution-treated or deformed by compression at temperatures above and below its β-*transus* to produce microstructures comprising martensitic, lamellar and globular α morphologies, as well as the existence or absence of β phase, and subsequently submitted to ageing treatments at 400°C/8h using in situ x-ray diffraction. Precipitated fractions of Ti_3Al were obtained via Rietveld refinement and aged microstructures were characterized by micro-hardness measurements. Results show that α_2 precipitation is favored by a globular morphology of α and hindered by a martensitic α morphology, and suggest that the presence of β phase also has as influence on precipitation.

Introduction

Ti-6Al-4V (composition in wt%) is the main representative of α+β alloys, responsible for more than 50% of all titanium alloys' applications. Reasons for its intensive application involve the equilibrium of properties such as strength, ductility, toughness and fatigue properties [1,2]. Although the alloy does not present an expressive response to ageing treatments when it comes to the precipitation of the α phase, the possibility of age hardening exists through the precipitation of intermetallic phase Ti_3Al (α_2), upon ageing at temperatures typically below 600°C [3].

Previous works on Ti-6Al-4V alloy have demonstrated that the driving force for α_2 formation depends on Al concentration in α phase, but also on oxygen concentration. Oxygen decreases the solubility limit of Al in α, facilitating the precipitation of Ti_3Al. This was verified for alloys with oxygen concentrations up to 0.22 wt% [3,4]. Precipitation of Ti_3Al is also assumed as consequence of Al segregation during rapid cooling, as suggested in previous works focused on the processing of the alloy and analogous systems via selective laser melting [5,6]. Additionally, a study of Ti_3Al precipitation in near-α Ti alloys has shown it occurs preferably at boundaries and dislocations at higher ageing temperatures, whereas a more homogeneous precipitation takes place at low temperatures [7].

The formation of coherent α_2 particles within α phase increases the yield stress and tensile strength of the alloy [8], but at the same time reduces its ductility [2]. In addition, as an ordered intermetallic phase, Ti_3Al-based systems present a combination of lightness and high temperature strength, despite its limited room-temperature ductility and toughness, which makes them interesting for the aerospace industry [9].

Within this context, the present work is presented, with the objective of studying the ageing behavior of Ti-64 alloy, focused on the precipitation of α_2 phase, with variation of the initial microstructure by a combination of heat treatments and thermomechanical processing. In situ synchrotron x-ray diffraction is used to keep track of phase evolution during ageing treatments.

Material and experiments

Material

The material used in this work was a Ti-64 alloy whose composition is given in **Table 1**. Its β-transus temperature, obtained via differential scanning calorimetry, was approximately 995°C.

Table 1. Composition of Ti-64 alloy used in this work

Element	Ti	Al	V	Fe	O	C	N	H
wt%	Bal.	6.03	4.18	0.24	0.14	0.013	0.011	0.006
[Al]eq	7.4			[Mo]eq	3.4			

Fabrication of initial conditions

The as-received billet presented a mill-annealed microstructure and therefore the alloy was submitted to a homogenization treatment at 1050°C/30 min. To remove any effects of prior thermomechanical processing. This fully recovered condition corresponds to one of the four initial conditions analyzed. **Figure 1** clarifies complete processing conditions used to produce each condition. For simplification purposes, each condition has been labeled according to treatment temperature ("1050" for 1050°C and "700" for 700°C) and type ("HT" for heat treatment and "D" for deformation with a strain rate of 10^{-1} s^{-1} up to a total strain of 0.5). Samples with 10 mm in diameter and 15 mm in length were cut from the billet with their length parallel to its length. Heat treatments were done in an EDG 10P-S furnace with argon 4.8 atmosphere and chamber temperature control and deformation by compression was carried out in a Gleeble® 3800 thermomechanical simulator with S-type thermocouples spot-welded to the specimens' surface for temperature control. All treatments were finished with water quenching.

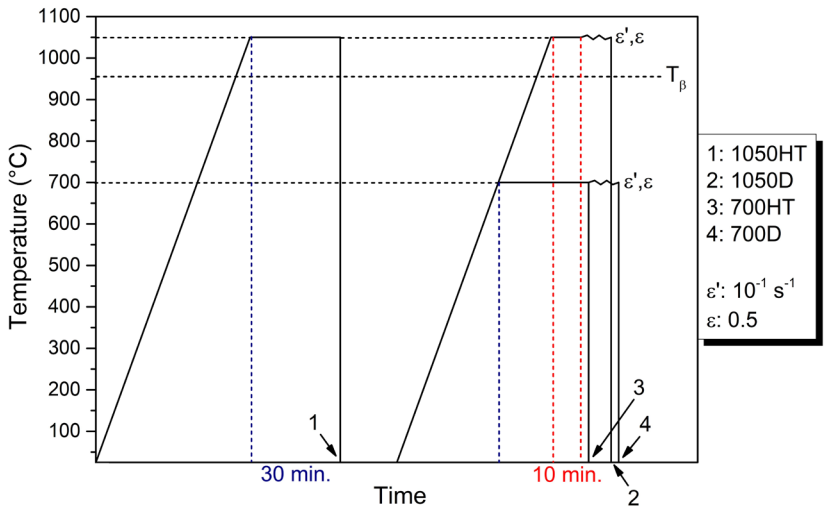

Figure 1. Schematic representation of procedures adopted to produce initial conditions (T_β: β-*transus*)

In situ x-ray diffraction

Samples with dimensions of 3×4×6 mm were cut from heat-treated and deformed specimens for in situ experiments. In the case of deformed specimens, samples were cut with their length parallel to the compression axis. Ageing treatments were done at the X-ray Scattering and Thermo-Mechanical Simulation (XTMS) experimental station of the XRD1 beamline at the UVX facility of the Brazilian Synchrotron Light Laboratory. Beam energy was 12 keV, with a corresponding wavelength of 1.0332 Å, and sample-to-detector distance was 325 mm. A Rayonix SX165 high resolution area detector with 39×39 μm^2 pixel size was used to acquire sections of Debye-Scherrer rings with a total exposure time of 60 s. Treatments were carried out in an adapted Gleeble® 3S50 thermomechanical simulator under vacuum levels of ~10^{-3} torr, and temperature was monitored by a K-type thermocouple spot-welded to the sample. To assure the

suppression of alpha case formation, the chosen treatment temperature was 400°C, with an ageing time of 8 h. During treatment, the detector was kept fixed at 2θ = 30°, which allowed the acquisition of a 2θ range between 15° and 45°. The probed surface was the 4×6 mm side of the sample. Acquired images were treated using Dracon software, a MATLAB® macro developed by the XTMS staff, to obtain the corresponding diffractograms, which were further quantitatively analyzed via Rietveld refinement [10,11] with MAUD [12] software.

Microstructural characterization

Pre-ageing microstructures were characterized via optical microscopy (OM) in a Zeiss Axio Scope.A1 microscope and scanning electron microscopy (SEM) in a FEI Inspect F50 microscope equipped with field emission gun using both secondary (SE) and backscattered (BSE) electrons' signal. Metallographic preparation involved an initial manual grinding step on sandpapers #320 and #600, an intermediate polishing step with a 3-µm diamond suspension and a final polishing step with a 90 vol% 0.04-µm OP-U – 10 vol% H_2O_2 solution. Polishing steps were carried out in a EcoMet 250 grinding/polishing machine.

Micro-hardness measurements

Vickers micro-hardness of both pre- and post-ageing microstructures was measured with a Leica VMHT-MOT tester with a load of 200 g. Ten measurements were collected randomly on the surface of samples prepared according to the procedure described above and the average values are hereby presented.

Results

Initial microstructures

In **Figure 2**, microstructures resulting from heat treatments and deformation are shown. For deformed conditions, compression direction corresponds to the vertical axis of images. With respect to heat-treated conditions, only the OM image of 1050HT is shown (**Figure 2a**) because there were not significant changes in microstructure at this scale after subsequent treatment at 700°C (700HT). In both cases, the microstructure is formed by coarse equiaxed prior β grains, with sizes in the order of 500 µm, within which α presents itself precipitated with a sharp martensitic morphology in the case of 1050HT condition (inset in **Figure 2a**) and with an intermediate lamellar morphology in 700HT (**Figure 2b**). Sample 1050D also presents a martensitic microstructure, with prior β grains elongated perpendicularly to the compression direction, as seen in the optical micrograph in **Figure 2c**. Finally, **Figure 2d** presents the microstructure obtained for 700D condition. In this case, α phase presents itself almost completely globular, but also with a remaining lamellar morphology. The micrograph of 700D condition is shown with BSE signal to improve the visualization of β phase along boundaries of α phase.

XRD results have confirmed that the starting microstructure of both 700D and 700HT conditions presented a mixture of α and β phases. Rietveld refinement analyses yielded fractions of 4.8 – 4.9 vol% β for both conditions, with an error of ~±0.1 vol%. Regarding 1050D and 1050HT conditions, both were expected to be composed solely by martensitic α' after water quenching from the β field; however, results of 1050D indicated the presence of β phase in this condition too, with an amount of 3.9 ± 0.9 vol%. On the other hand, 1050HT was purely martensitic. **Figure 3** shows the 2D images containing sections of Debye-Scherrer rings acquired at room temperature, before heating to 400°C. In addition to the pure indication of phases' presence or absence, the rings also provide information regarding granulometry, since **Figure 3d** shows continuous rings that indicate refinement of α phase's grains, in contrast to the other conditions, with preferential orientations given by the coarseness of prior β grains.

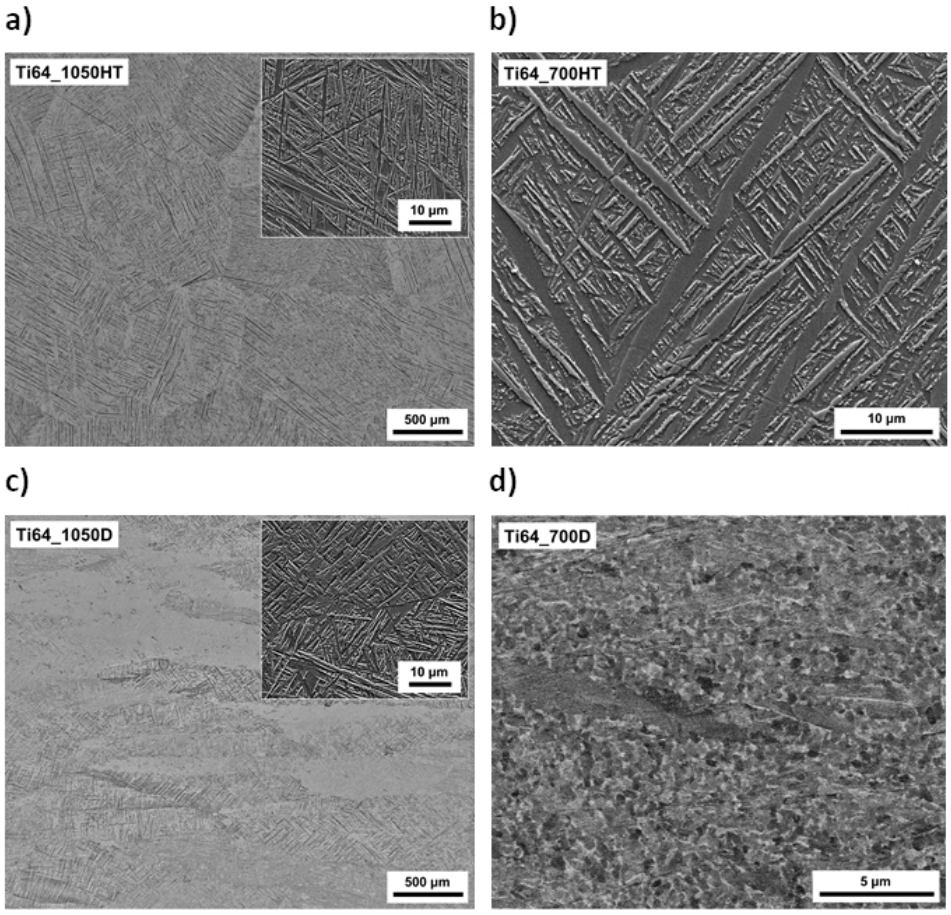

Figure 2. a) Optical (main) and SE-SEM (inset) images of 1050HT condition; b) SE-SEM image of 700HT condition; c) optical (main) and SE-SEM (inset) images of 1050D condition; d) BSE-SEM image of 700D condition

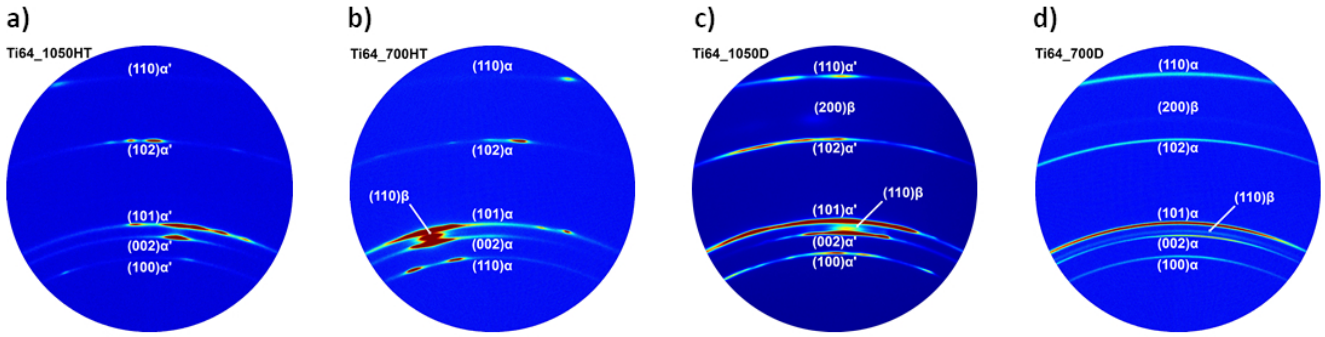

Figure 3. Sections of Debye-Scherrer rings acquired at RT for a) 1050HT; b) 700HT; c) 1050D; d) 700D

Precipitation of Ti_3Al during ageing

Figure 4 presents the evolution of diffraction peaks throughout ageing treatments. During heating to 400°C, no significant changes were observed other than an increase of lattice parameters, which is expected due to thermal expansion of the material. It is important to emphasize that focus was given to α_2 reflections which were easier to visualize individually in the images due to their 2θ position, namely $(002)\alpha_2$ and $(202)\alpha_2$. However, there is superposition of several α_2 reflections with both α and β reflections, as is the case shown in **Figure 4** for $(201)\alpha_2$, superimposed between (110)β and (101) α/α' reflections, and also for $(200)\alpha_2$ reflection, which is superimposed with (100)α/α' reflection. From the images, based on the amount and intensity of visible peaks, it is possible to observe a clear higher tendency of precipitation in the 700D condition. On the other hand, 1050HT and 1050D conditions presented a relatively

hindered precipitation. Quantitative analysis of diffractograms provided the evolution of phase fractions throughout ageing (R_{wp} ≤ 10.5%). **Table 2** summarizes the amounts of each phase at the end of treatment at 400°C.

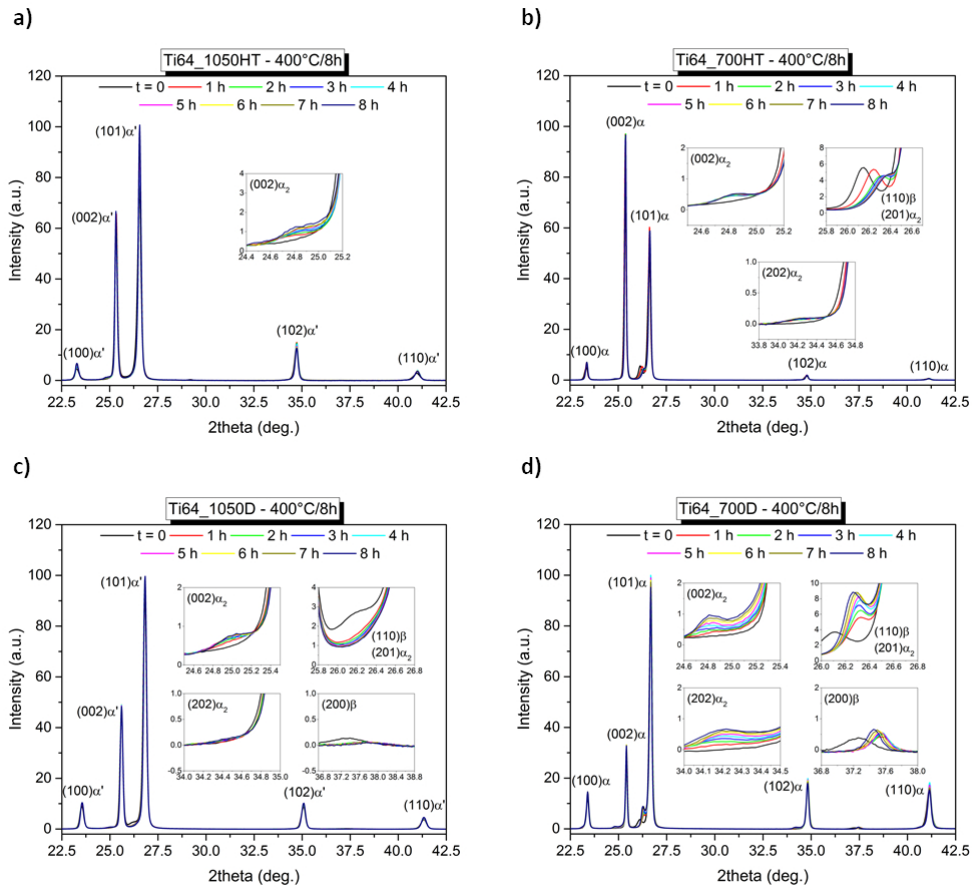

Figure 4. Evolution of reflections during ageing for a) 1050HT; b) 700HT; c) 1050D; d) 700D

Table 2. Phase fractions obtained for each condition after ageing at 400°C/8h

Condition	1050HT	1050D	700HT	700D
Vol% α	92.4	90.5	87.3	83.8
Vol% β	-	-	3.9±0.6	5.7±0.5
Vol% α_2	7.6±1.1	6.9±1.2	8.8±0.8	10.5±2.2

Discussion

From results shown in **Table 2**, it is possible to observe that 700D condition, with a mostly globular α morphology, has precipitated the highest amount of α_2, followed by 700HT, with a partially lamellar α morphology. Martensitic conditions – 1050D and 1050HT – have precipitated the smallest amounts of this said phase. Zhang and Li studied the precipitation of Ti_3Al in near-α alloys with bimodal microstructure and have observed that it may occur in a heterogeneous manner, preferably at phase boundaries and dislocations in lamellar α phase and homogeneously within primary globular α, due to strong aluminum partitioning to the latter [7]. Similar results had already been obtained by Lütjering and Weissmann [13]. Additionally, in comparison with binary Ti-Al alloys, the misfit between α and α_2 in alloys with more complex compositions is be larger, which makes α_2 nucleation more difficult and therefore with a tendency to form heterogeneously [14].

Based on final fraction results, precipitation kinetics was evaluated via Johnson-Mehl-Avrami-Kolmogorov (JMAK) equation [15-17] for the extreme conditions, i.e. for condition with maximum and minimum Ti_3Al precipitation: 700D and

1050D, respectively. **Figure 5** depicts plots of $\ln(\ln(^{1}/_{1-x}))$ as function of ln(t), where "x" is α_2 phase fraction and "t" is ageing time, for both conditions. Through linear interpolation of points, it was possible to obtain the slope of the curves, which corresponds to the "n" value in Avrami's equation. For 700D, "n" equals to 0.76±0.02 and, for 1050D, "n" equals to 1.06±0.06. Considering long-range diffusion controlled transformation, a "n" value between 0.5 and 1, the case of "700D" condition, indicates growth between one dimension (n = 0.5) and two dimensions (n = 1) [18,19], which would result in particles shaped as elongated disks [20]. A value of n ≃ 1, case of "1050D" condition, indicated two-dimensional growth.

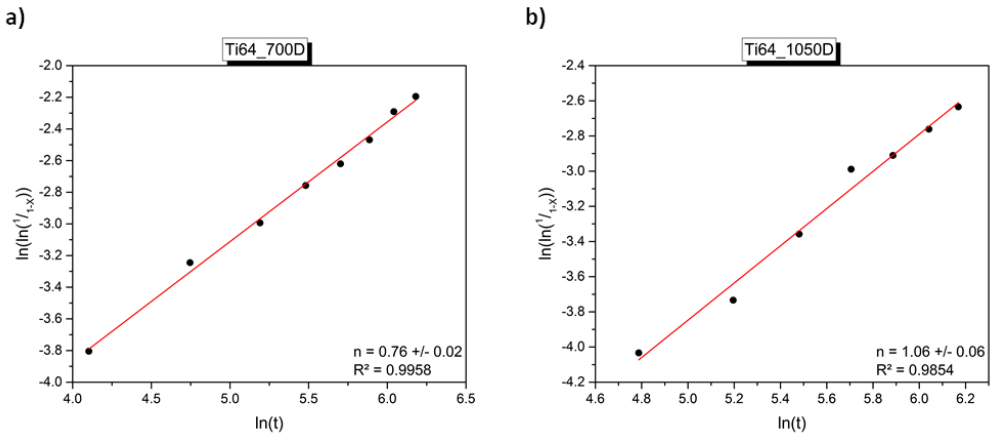

Figure 5. Avrami's plot of α_2 precipitation for a) 700D and b) 1050D conditions

As expected, the hardness of Ti64 alloy in all conditions has increased after ageing. **Table 3** shows micro-hardness results before and after ageing. These results run in parallel to quantitative analysis results, indicating that the higher the amount of α_2, the higher the hardness increase. It is possible to observe that no significant increase in hardness was observed, again due to treatments' low temperature and short time. However, the present results are useful to indicate the tendency of the hardening effect of α_2 phase on the alloy's mechanical properties. Previous studies have evaluated the effect of α_2 precipitation on mechanical properties of Ti-64 alloy and an increase in yield and tensile strength has been observed, but with a negative effect in the alloy's ductility and fatigue behavior [8,21]. However, a non-uniform dispersion of the phase appears to have a less deleterious effect on ductility [14].

The effect of β phase can be evaluated by comparing 1050HT and 1050D conditions. Since 1050D presented a certain amount of β at the beginning of treatment and a smaller amount of α_2 at the end of treatment, it might be suggested that the presence of a second phase affects the composition of α phase, making it leaner in Ti and Al in comparison to its composition as a sole phase in the material, and this could retard Ti_3Al formation. However, because the difference between final α_2 amounts is not so expressive when error values are taken into account, this might be a secondary effect, especially because, as seen in **Figure 4**, β peaks disappear in the initial moments of ageing, indicating it decomposed into α.

Table 3. Average micro-hardness values obtained for each condition before and after ageing at 400°C/8h

Condition	1050HT	1050D	700HT	700D
Pre-ageing hardness (0.2 HV)	387.3±5.1	383.9±7.5	384.3±4.8	378.5±5.3
Post-ageing hardness (0.2 HV)	397.7±5.8	392.6±5.6	396.7±5.1	391.9±6.6
Hardness increase (%)	2.7	2.3	3.2	3.5

Conclusions

The precipitation of intermetallic phase Ti_3Al in Ti-64 alloy with different starting microstructures during ageing at 400°C/8h was evaluated. XRD results indicate and micro-hardness measurements further corroborate that precipitation is favored by a globular morphology of α phase. The presence of β phase also appears to play a role on precipitation kinetics

through its effect on the composition of α phase. Low hardness variations are results of low temperature and short ageing times, but overall the obtained results are useful to indicate tendencies in the alloy's behavior upon ageing with respect to the intermetallic's precipitation.

Acknowledgements

CNPEM's staff is acknowledged for the assistance provided during thermomechanical treatments and in situ ageing treatments. This work was funded by the National Council for Scientific and Technological Development in Brazil and supported by the International Cooperation Program PROBRAL CAPES/DAAD, financed by CAPES – Brazilian Federal Agency for Support and Evaluation of Graduate Education within the Ministry of Education of Brazil.

References

[1] C. Leyens, M. Peters, *Titanium and Titanium Alloys*, Wiley-VCH, 2003.

[2] G. Lütjering, J. C. Williams, *Titanium*, Springer, 2007.

[3] R. Boyer, G. Elsch, E. W. Collins, *Materials Property Handbook: Titanium Alloys*, ASM International, 1994.

[4] G. Welsch, W. Bunk, *Metall. Trans. A* 13 (1982) 889-899.

[5] L. Thijs et al., *Acta Mater.* 58 (2010) 3303-3312.

[6] P. Barriobero-Vila et al., *Materials* 10 (2017) 1-14.

[7] J. Zhang, D. Li, *Mat. Sci. Eng. A* 341 (2003) 229-235.

[8] Z. Wu et al., *Metall. Mater. Trans. A* 44 (2013) 1706-1713.

[9] S. Banumathy, P. Ghosal, A. K. Singh, *J. Alloy. Compd.* 394 (2005) 181-185.

[10] L. B. McCusker et al. *J. Appl. Crystallogr.* 32 (1999) 36-50.

[11] H.-R. Wenk et al. *Powder Diffr.* 29 (2014) 220-232.

[12] MAUD: Materials Analysis Using Diffraction, available on http://maud.radiographema.eu/.

[13] G. Lütjering, S. Weissmann, *Acta Metall.* 18 (1970) 785-795.

[14] I. Polmear et al. *Light Alloys: Metallurgy of the Light Metals*, Elsevier, 2017.

[15] A. N. Kolmogorov, Izv. *Akad. Nauk. SSSR Ser. Mat.* 1 (1937) 355-359.

[16] W. A. Johnson, R. F. Mehl, *Trans. Am. Inst. Min. Metall. Eng.* 135 (1939) 416-458.

[17] M. Avrami, *J. Chem. Phys.* 9 (1941) 177-184.

[18] J. W. Christian, *The Theory of Transformations in Metals and Alloys*, Pergamon, 2002.

[19] S. Banerjee, P. Mukhopadhyay, *Phase Transformations: Examples from Titanium and Zirconium Alloys*, Elsevier, 2007.

[20] G. A. Young, D. R. Eno, *Long range ordering in model Ni-Cr-X alloys*, Fontevraud 8: Conference on Contribution of Materials Investigations and Operating Experience to LWRs' Safety, Performance and Reliability, France, 2015.

[21] S. Hémery, P. Villechaise, *Scripta Mater.* 130 (2017) 157-160.